Journal of Industrial and Engineering Chemistry 159 (2026) 777–786

Contents lists available at ScienceDirect

Journal of Industrial and Engineering Chemistry

journal homepage: www.elsevier.com/locate/jiec

Full Length Article

Decolorization of reactive Red 120 by a novel hybrid hydrodynamic cavitation and non-thermal plasma reactor

Mojca Zupanc [a], Sebastian Dahle [b], Matevž Dular [a], Gregor Primc [c], Rok Zaplotnik [c], Martin Petkovšek [a,*]

[a] Faculty of Mechanical Engineering, University of Ljubljana, Aškerčeva 6, Ljubljana, Slovenia
[b] Biotechnical Faculty, University of Ljubljana, Jamnikarjeva 101, Ljubljana, Slovenia
[c] Department of Surface Engineering, Jožef Stefan Institute, Jamova cesta 39, Ljubljana, Slovenia

ARTICLE INFO

Keywords:
Advanced oxidation processes
Hydrogen peroxide
Azo dye
Removal
Hydrodynamic cavitation
Gaseous plasma

ABSTRACT

The treatment of dye-contaminated wastewater remains a significant challenge for environmental management due to the high stability and persistence of many azo dyes. The purpose of this study was to develop and evaluate a novel hybrid rotor–stator hydrodynamic cavitation non-thermal plasma device designed to enhance the decolorization of Reactive Red 120. The configuration integrates atmospheric-pressure plasma directly into a cavitating flow field, attempting to increase gas–liquid interfacial contact and promote mass transfer of reactive species into the liquid. The device performance was investigated by assessing the effects of various parameters on H_2O_2 production, pH, conductivity, and energy consumption. The results show generation of reactive species at all tested parameters, with higher H_2O_2 production in deionized compared to tap water. Rotational speed, discharge voltage and air flow rate all influenced H_2O_2 production and the highest concentration achieved was 9.9 mg/L in 15 min. Decolorization was evaluated at three initial concentrations and followed apparent pseudo first-order kinetics, with higher degradation rates observed at lower initial dye concentrations (0.0273, 0.0234 and 0.0168/min at 25, 50 and 100 mg/L, respectively). The study demonstrates that coupling of hydrodynamic cavitation with non-thermal plasma produces synergistic effects and has potential to treat complex wastewaters.

Introduction

The growing presence of pollutants in aquatic environment poses a serious and escalating threat to global water resources. Critical contaminants include pharmaceuticals, personal care products, pesticides, and synthetic dyes, the latter extensively used in textile, leather, paper, cosmetics, food and polymer industries [1,2]. Industrial wastewater (WW) is a major contributor to water pollution due to its complex composition and high content of toxic, non-biodegradable compounds [3,4], with textile dyeing effluents contributing approximately 17–20 % of global industrial WW. The textile sector consumes roughly 70,000 tonnes of dyes annually, of which up to 20 % is lost during processing [4], making it the second-largest polluter of clean water after agriculture [5]. Azo dyes, often detected at concentrations up to 200 mg/L [6,7], are of particular concern due to their complex molecular structure, high solubility and persistence [2,3,8]. Even at low concentrations, these colourants can be toxic to aquatic organisms, inhibit photosynthesis, deplete dissolved oxygen, and bioaccumulate in food chains [9–11]. Their effective removal before discharge is therefore an urgent ecological necessity.

In recent years, advanced oxidation processes (AOPs) such as hydrodynamic cavitation (HC) and non-thermal atmospheric-pressure plasma have gained attention for degradation of refractory azo dyes [12–15]. These methods offer advantages over adsorption, coagulation, and biodegradation, as they prevent merely the transfer of pollutants between phases, thus minimizing sludge generation [4,7]. HC involves rapid pressure fluctuations in a liquid that create vapor cavities that, upon collapse, release energy locally, triggering chemical (formation of $^{\bullet}OH$) and mechanical (i.e., extreme shear forces, microjets, and shock-waves) effects that can enhance pollutant degradation and mass transfer [16]. Non-thermal plasma, by contrast, produces energetic photons, radicals, electrons, ions, and UV radiation, as well as various excited and reactive species including O_3, NO_x and $^{\bullet}OH$ [17–19]. Pollutant degradation occurs at the gas–liquid interphase through short-lived species (when using air plasma) such as $HO_2^{\bullet}$, $^{\bullet}OH$, NO_2 or in the bulk liquid via long-lived oxidants like O_3, H_2O_2, and NO_3^- [13,17–21].

* Corresponding author.
E-mail address: martin.petkovsek@fs.uni-lj.si (M. Petkovšek).

https://doi.org/10.1016/j.jiec.2026.03.008
Received 11 February 2026; Received in revised form 3 March 2026; Accepted 9 March 2026
Available online 10 March 2026

Mostly investigated HC systems can be classified as static (throttling) or dynamic [14,22–24]. Static devices such as orifice plates, Venturi tubes and swirling jet-induced HC systems, generate cavitation through flow constriction, whereas dynamic devices like rotor-rotor or rotor–-stator generators, produce cavitation through mechanical motion and shear forces. Plasma systems, in turn, are categorized by plasma generation location and include gas-phase discharges above or near the water surface [7,11,25], liquid-phase discharges generated within the liquid [6], and gas–liquid hybrid phase discharges, where plasma is ignited in gas bubbles either inside the liquid or remotely before re-entry [8,20]. Common discharge types include dielectric barrier discharge (DBD) systems [5], corona discharges (CD) [13], and plasma jets (e.g. gliding arc jets, DBD jets, radio-frequency plasma jets) where plasma generated in a reactor or nozzle is directed toward the medium as a gaseous stream of excited species[8,25,26].

Although both cavitation and plasma exhibit strong oxidation capabilities, each has intrinsic limitations when applied individually. Consequently, several studies have explored their coupling in different configurations [15,27–33]. Nevertheless, as short-lived reactive species reside at the gas–liquid interface for extremely short time periods [19], further optimization of the mass transfer of plasma-generated species into the bulk liquid remains necessary [20]. To try and address this, the present study: i) introduces, for the first time, a novel hybrid system integrating a rotor–stator cavitation-plasma (RSC-PL) device, ii) systematically investigates the influence of the water matrix, rotational speed, air flow rate, and discharge voltage on pH, conductivity, H_2O_2 formation and energy consumption, and iii) evaluates, for the first time, the decolorization and reaction kinetics of the azo dye Reactive Red 120 (RR120) in a RSC-PL device at different initial concentrations, along with the overall energy efficiency under selected conditions.

Materials and methods

Chemicals

Reactive Red 120 (RR120 $\geq$ 50 %) was purchased from Sigma-Aldrich, Merck KGaA (Darmstadt, Germany). Potassium phthalate monobasic ($C_8H_5KO_4$ $\geq$ 99.5 %), ammonium molybdate tetrahydrate ($(NH_4)_6Mo_7O_{24}{\cdot}4H_2O$ $\geq$ 99 %) and NaOH used for the potassium iodide (KI) method were all purchased from Sigma-Aldrich Merck KGaA (Darmstadt, Germany), while KI was purchased from Honeywell Fluka (Seelze, Germany). 30 % (v/v) H_2O_2 was procured from Roth (Karlsruhe, Germany).

Development of a novel cavitation-plasma device

Non-thermal plasma treatment is often constrained by the limited transfer of reactive gas species within plasma-liquid systems. It has been reported that the lifetime of the most crucial radical species formed in the gas phase, $^{\bullet}OH$, is approximately 3.7×10^{-9} s and its diffusion into the bulk solution is around 6×10^{-9} m [18,34]. Therefore, the reactor design plays a pivotal role, as both the plasma generation approach and the electrode configuration govern the production of reactive species and their transfer into the liquid. Previous studies have shown that cavitation can produce synergistic effects when combined with plasma. For example, Fang et al., 2019 [35] demonstrated that acoustic cavitation enables spark discharge breakdown at 24 times higher conductivities because numerous cavitation bubbles facilitate plasma discharge propagation between electrodes. Similarly, Pereira et al., 2023 [34] reported that HC bubbles provide conductive pathways for glow plasma discharge, with the resulting synergy enhancing $^{\bullet}OH$ generation, UV emission, and shock waves that drive pollutant degradation. In a plasma-HC hybrid systems based on self-excited oscillation structures, Song et al., 2024 [15] and Nie et al., 2022 [36] showed that a high-speed jet beam entering the cavitation chamber generates intense turbulence, thickening the shear layer and ensuring thorough mixing of oxidizing plasma-generated species with the liquid sample. The present study introduces a novel cavitation-plasma device designed to further enhance the interfacial area between the plasma and liquid phase by integrating a rotor–stator HC unit with an in-situ plasma discharge. By injecting the air plasma afterglow directly into the rotor–stator system, the interfacial area (surface-to-volume ratio) between plasma gas and water is substantially increased. The design of gas distribution was focused on uniform gas dispersion along all 10 electrodes with the idea to deliver gas into the treatment chamber as large bubbles which would be fragmented by shear forces generated by the rotor–stator geometry. The plasma discharge itself is ignited directly onto the water sample surface as the air stream enters the HC unit, thereby minimizing any dwell time occurring in other remote plasma setups. The resulting reactive oxygen and nitrogen species (RONS) rich gas bubbles are dispersed throughout the sample and subsequently collapse under HC conditions, generating intense micro-mixing and promoting effective transfer of reactive species into the bulk solution. This hybrid design aims to couple high reactive species yield of plasma with the dynamic collapse of cavitation bubbles to overcome mass-transfer limitations. Given the strong spatiotemporal constraints inherent to both processes, ensuring that contaminants continuously encounter RONS within the active cavitation-plasma treatment zone is essential for maximizing treatment effectiveness and efficiency.

Experimental setup of the novel RSC-PL device

The experimental setup of this novel hybrid system is presented in Fig. 1. RSC-PL consists of a rotor–stator cavitation device (1) with integrated non-thermal plasma inside the treatment chamber. The device is driven by a 1.5 kW electric motor, connected to a closed circuit with a 7 L reservoir (2). All parts that are in contact with the sample are made from stainless steel, except the stator, which is fabricated from transparent acrylic glass to ensure visual transparency of the treatment chamber. To maintain a constant temperature of the treated sample, a cooling coil (3) was installed in the reservoir and connected to the DuraChill external portable cooling unit with a cooling capacity of 1.28 kW. The temperature was monitored using a K-type thermocouple (4) installed directly in the reservoir. The HC unit features a serrated 12-tooth rotor with 50 mm in diameter facing in axial direction to a 10-tooth stator (5), setting a gap of 2 mm between them. Rotor's teeth have inclination of 10.7°, while stator teeth are flat with grooves of 3 mm in width and 2 mm in depth. Water flow rates were experimentally determined using a volumetric principle for each operating condition.

The non-thermal plasma unit features an additional 10 hollow brass electrodes with an outer diameter of 4 mm, an inner diameter of 3 mm, and a length of 55 mm (6), equally distributed in a circular arrangement with the electrodes' centres 20 mm from the centre of the stator, installed in axial direction through the stator with 0.5 mm indented from the stator's inner surface, presenting the high voltage (HV) electrode. For the grounded electrode, a stainless-steel rotor was used, such that the electrical discharge ignited onto the water sample surface through the gas stream during bubble formation. It was electrically grounded through the housing of the treatment chamber via rotor shaft bearing. The hollow HV electrodes in the stator were connected to a Fourier synthesis high voltage pulse generator (S/N 040–7, Ing.-Büro Jürgen Klein, Germany) (7) supplying alternating HV pulses with a full width at half mean of 0.6 μs and a possibility of adjusting pulse repetition frequency (0–30 kHz) and amplitude (5–20 kV). The HV pulse generator's storage capacitor of 200 pF yields pulse energies corresponding to the pulse amplitude of 2.5–40 mJ, respectively. For the purposes of this study, only air was used as the discharge gas.

Performance characterization of the RSC-PL device

Plasma characterization

Optical emission spectroscopy (OES) was used to measure the light

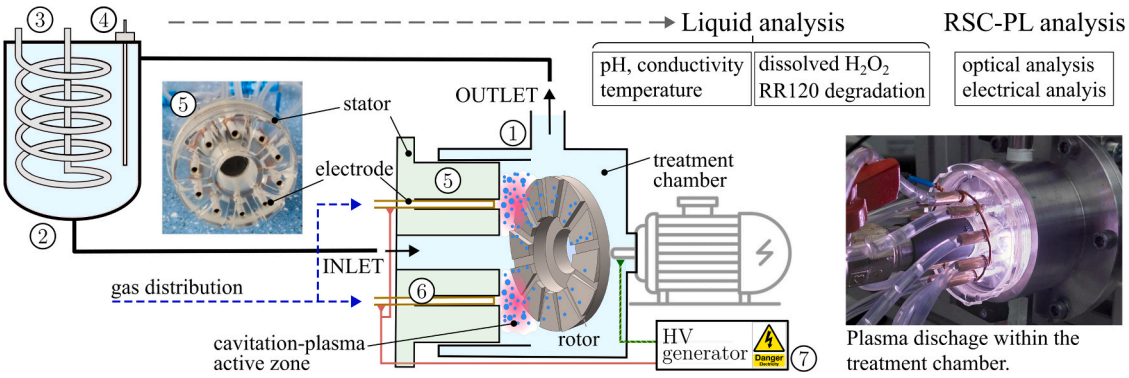

Fig. 1. Experimental setup scheme – (1) RSC-PL device, (2) reservoir, (3) cooling coil, (4) thermometer, (5) stator, (6) hollow stator electrodes, (7) high-voltage power supply.

emitted by plasma. Due to its non-invasive nature, OES is currently the only method suitable for measuring plasma parameters in the present experimental setup. The measurements were performed separately on a single active electrode. An AvaSpec-3648 spectrometer (Avantes, Netherlands) with a spectral resolution of 0.5 nm in a wavelength range of 200–1100 nm was used. The collimating lens was mounted directly on the RSC-PL device, observing the plasma generation region through the acrylic stator body, and connected to the spectrometer via an optical fiber. The integration time varied between 10 and 1000 ms. Power consumption measurements are described in section 2.4.5. The oscilloscope measurements were also used to calibrate the HV pulse generator's peak output voltage and pulse repetition rate (see Suppl. 1). We used P6015A Tektronix high voltage probe connected to LeCroy WaveRunner HRO 66Zi oscilloscope.

H_2O_2 production measurements

Since H_2O_2 usually serves as an indicator of plasma oxidation potential, its generation is commonly measured for initial assessment and comparison of performance of the plasma device. For the purposes of this study, the formation of H_2O_2 in the RSC-PL device was determined in tap and deionized water (TW and DW). The time-dependent measurements of H_2O_2 concentrations were performed using the KI method [37]. Briefly, 0.3 mL of samples were mixed in a 4 mL cuvette with 0.75 mL of reagent A (0.1 M $C_8H_5KO_4$), 0.75 mL of reagent B (0.4 M KI, 0.06 M NaOH, $\approx 10^{-4}$ M $(NH_4)_6Mo_7O_{24}{\cdot}4H_2O$), and 1.2 mL DW. After mixing, the maximum absorbance peak was measured at 352 nm using a UV–Vis DR3900 spectrophotometer (Hach). H_2O_2 concentrations were then determined from a calibration curve in the range of 0.0162–8.0 mg/L, which showed excellent linearity ($R^2 = 0.9995$) (Suppl. 2). Samples were diluted when necessary to fall within the calibration curve's range. The sampling, during which cavitation and plasma units were shut down, was performed simultaneously with the sampling for the measurements of conductivity and pH.

pH and conductivity measurements

The physico-chemical changes of samples due to formation of RONS during plasma-cavitation treatment, were determined before, during and after experiments. For this purpose, conductivity and pH were measured using Hach HQ430d multimeter with an interchangeable IntelliCAL PHC725 electrode and CDC401 probe, respectively. These samples were returned to the reactor after measurements.

Dye decolorization measurements

The effectiveness of the RSC-PL device was determined for RR120. The experimental conditions (DW, rotor's frequency of 10800 rpm, air flow of 10 L/min and discharge voltage of 6.7 kV) producing the highest amount of H_2O_2 were selected for these experiments. A fresh solution of the dye was prepared before each experiment by dissolving the powdered RR120 in DW to obtain the desired concentrations. The pH of the samples before the experiments was not adjusted and remained at its initial value (Suppl. 7: from 6.8 to 7.1), hereafter referred to as neutral pH. Initial, intermediate, and final dye concentrations were calculated from a calibration curve plotted in the range of 0.782–100 mg/L ($R^2 = 1$) by measuring absorbance at 513 nm (Hach DR3900) (Suppl. 3). The removal effectiveness (R) was calculated using the following Eq. (1):

$$(R\%) = \left[\frac{C_0 - C}{C_0}\right] \times 100 \quad (1)$$

The first-order kinetic best fitted the degradation of RR120, which can be described by the following equation Eq. (2):

$$\ln\left(\frac{C}{Co}\right) = -kt \quad (2)$$

where C is the remaining concentration of RR120 (mg/L), C_0 is the initial concentration of RR120 (mg/L), t is the treatment time (min), and k is the first-order degradation rate constant (min^{-1}).

Energy consumption and yield measurements

To evaluate the efficiency of the novel RSC-PL device for H_2O_2 production and RR120 removal, energy consumption measurements were performed. The energy consumption of the plasma and cavitation units under the experimental conditions investigated (Tables 1 and 2) was measured separately by monitoring power over time. The cooling unit was not included in the power analysis. Specifically, the power of the rotor–stator cavitator (P_{RSC}) and the power of the HV power supply (P_{PL}) were recorded using a Norma 4000 Power Analyzer (Fluke, Netherlands).

The competitiveness of novel cavitation-plasma devices depends on energy use, energy yield (Y), defined as the ratio between the amount of H_2O_2 produced or RR120 removed during treatment, and the energy

Table 1
Investigated experimental conditions for determination of the effect of the RSC-PL device on H_2O_2 generation, pH, conductivity, and energy consumption.

Exp.	Water matrix	Sampling (min)	Np^*[a]	n (rpm)	Q_{water} (L/min)	Q_{air} (L/min)	U (kV)
1	TW	0, 2.5, 5,	17	10,800	4.6	10	6.7
2		10, 15	15	6000	4.0		
3			13.5	3000	3.6		
4	DW	0, 2.5, 5,	17	10,800	4.6	10	6.7
5		10, 15	15	6000	4.0		
6			13.5	3000	3.6		
7	DW	0, 2.5,	15.5	10,800	4.2	12.5	6.7
8		5,10, 15	13		3.5	15	
9	DW	0, 2.5,	17	10,800	4.6	10	4.1
10		5,10, 15			4.6		3.0

[a] Np^*: denotes the total number of liquid passes through the active cavitation-plasma zone corresponding to a 15-min treatment.

Table 2
Investigated operating parameters for decolorization of RR120.

Exp.	Watermatrix	RR120 (mg/L)	Sampling(min)	*Np*	*n* (rpm)	Q_{water} (L/min)	Q_{air} (L/min)	*U* (kV)
A*	DW	100	0, 2.5, 5, 10, 15, **30**	17	10,800	4.6	10	6.7
B*		50						
C*		25						
D			0, 2.5, 5, 10, 15, **30**	15	6000	4.0		
E				13.5	3000	3.6		

* experiments performed in triplicate; 30 min: refers to the "resting period", during which the samples were removed from the reactor and left to assess the RR120 concentration post-treatment.

consumed. The calculation of *Y*-values presents the energy needed for maximum H_2O_2 production (Y_{H2O2}) and dye removal (Y_{RR120}) as shown in Eqs. (3) and (4), respectively:

$$Y_{H2O2}(mg/Wh) = \frac{C_{max}V}{Pt} \quad (3)$$

$$Y_{RR120}(mg/Wh) = \frac{C_0VR}{Pt} \quad (4)$$

C_{max} (mg/L) is the maximum concentration of the H_2O_2 formed, *V* (L) is the volume of the treated sample, $P = P_{RSC} + P_{PL}$ (W) is the power needed for the maximum removal of RR120 or production of H_2O_2, *t* (s) is the time required to achieve this removal, C_0 (mg/L) is the initial concentration of the dye, and R the fraction of RR120 removed.

Experimental design

The overview of the experimental conditions is provided in Tables 1 and 2. Parameters kept constant for all experiments were the following: sample volume (4 L), pH (neutral), rotor–stator geometry (see Section 2.2), HV pulse repetition rate (10.8 kHz), sample temperature (25 ± 2 °C), and sampling intervals (0, 2.5, 5, 10, 15, and 30 min). A time sequence up to 15 min represents the treatment period using the RSC-PL device, after which the sample was removed and left at room temperature for an additional 15 min ("resting period") to evaluate post-cavitation-plasma treatment changes, in case of RR120 concentration measurements. The effectiveness of RSC-PL was investigated by changing discharge voltage (3, 4.1 and 6.7 kV), rotational speed (3000, 6000 and 10800 rpm) and air flow rate (10, 12.5 and 15 L/min), the last two influencing flow rate of the sample Q_{water}.

The performance of the novel RSC-PL device was evaluated in two stages: (i) assessment of experimental conditions on pH, conductivity, H_2O_2 generation, and energy consumption (Table 1: Exps. 1–10) and (ii) decolorization of the azo dye RR120 (Table 2: Exps. A–E). In the first stage, the effects of water matrix, rotational speed *n*, air flow rate Q_{air}, and an amplitude of a discharge voltage peak *U* were systematically investigated (Table 1). All three have been previously found to influence the generation of the reactive species.

In the second stage, the effectiveness of the RSC-PL device was first assessed under optimal experimental conditions for H_2O_2 generation determined in the first stage (Exp. 4). For these experiments (Table 2: Exps. A–C), three environmentally relevant RR120 concentrations (25, 50, and 100 mg/L) were selected. To assess the repeatability of the treatment, these experiments were performed in triplicate, and the results are reported as mean ± standard deviation values. Secondly, to determine the best balance between effectiveness and energy use, the decolorization of 25 mg/L of RR120 was also evaluated at rotational speeds of 6000 and 3000 rpms (Table 2: Exps. D–E).

In addition, two control experiments (Suppl. 4: Exps. C1–C2) were performed to confirm that the RR120 decolorization during cavitation-plasma treatment occurs primarily due to the short-lived species formed. In C1, the effect of HC with the addition of the highest amount of H_2O_2 formed during Exp. 4 on RR120 decolorization was evaluated. Whereas in C2, the sole effect of H_2O_2 on decolorization was assessed using a magnetic stirrer.

Results and discussion

RSC-PL device characterization

Plasma characterization

Plasma species generated within the active zone (shown in Fig. 1) were determined in-situ using an optical emission spectrometer (OES). The typical OES spectrum of the air plasma generated in an RSC-PL device is presented in Fig. 2A and the typical voltage waveform of the HV pulse is presented in Fig. 2B.

The first notable observation is that the recorded OES spectrum differs significantly from the typical optical emission spectra generally reported for air atmospheric plasmas interacting with water. The usual spectrum, presented in many works [3,5,11] consists of N_2 second positive (C-B) system, OH 306 nm system, N_2^+ first negative (B-X) system, and NO_γ bands. When air plasma is generated at reduced pressures, the N_2 first positive system (B-A) also becomes observable, and under sufficiently low-pressure conditions, it often becomes the dominant spectral feature [38]. However, in Fig. 2A, none of these spectral features can be observed. The spectrum is more similar to laser-induced air plasma [39].

The highest peak in the OES spectrum is the hydrogen Balmer alpha peak at 656 nm. There are also other emission peaks that are associated with neutral atom transitions of O and N atoms. These atomic emission lines of neutral atoms suggest a very high dissociation fraction of nitrogen, oxygen, and water molecules, which is supported by the fact that there are no molecular transitions observed. The plasma is quite powerful, because besides a practically 100 % dissociation fraction, the dissociated atoms are further ionized, as evidenced by the presence of atomic ion emission lines (N^+ and O^+).

The atomic emission lines are significantly broadened, indicating a high plasma density. From Stark broadening of hydrogen Balmer emission lines, especially H_α, we estimated an electron density of approximately $2 \times 10^{24}/m^3$. Such a high electron density is typical for atmospheric-pressure streamer plasmas, particularly in short, high-power excitation pulses like those used in our setup. An approximation of the electron temperature was also determined from OES measurements with the use of Boltzmann plot. The electron temperature was below 1 eV, whereas the gas temperature was slightly above room temperature, which is typical for such short-pulsed plasmas.

The presence of copper and zinc emission lines proves the sputtering of metals from the electrodes. However here it should be stressed, that the OES was recorded through the metal tube electrodes, which explains the presence of Zn and Cu lines in the spectra. The associated sputtering is confined to the inner surface of the tubes, where redeposition of Zn and Cu also occurs, and no deposition was observed elsewhere. Moreover, the emission intensity of these metals is very low, indicating that Zn and Cu do not significantly affect the plasma treatment of the liquid in our experiment.

Based on the OES spectrum (Fig. 2A), the plasma has a high dissociation fraction, which is why mostly dissociated atoms are detected. These unstable atoms subsequently recombine into stable molecules. Since no emission from OH molecules is detected within the plasma region, this indicates that OH molecules, and consequently also H_2O_2,

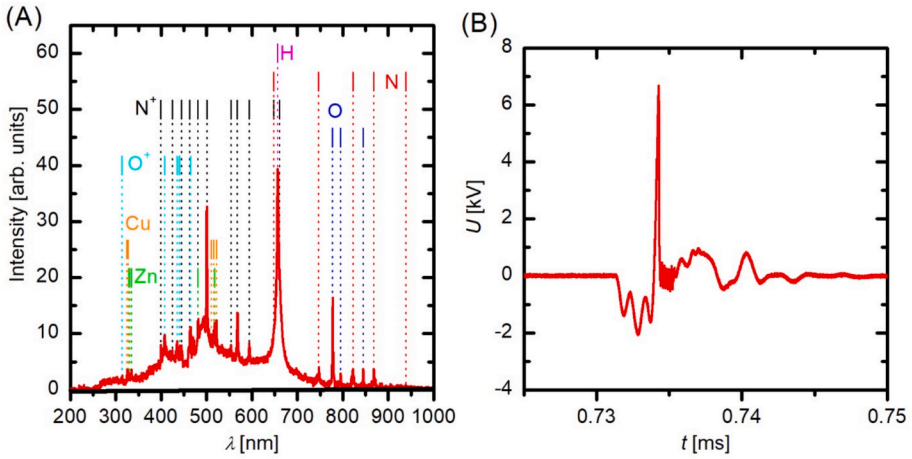

Fig. 2. The OES spectrum (A) and the voltage waveform (B) of the air RSC-PL plasma generated at a pulse repetition frequency of 10.8 kHz and power of 297 W, 10800 rpm, and 1 L/min of air inlet (on a single electrode).

are formed primarily in the afterglow region near the water surface, through various different reactions [40]. Since the OH molecules are located in the afterglow region and are not electronically excited, they do not emit light and therefore cannot be detected by optical emission spectroscopy. If some of these molecules diffuse back into the plasma region, they are not simply excited, rather, due to the high plasma power, they are dissociated into hydrogen and oxygen atoms again.

A short high voltage pulse that generates the plasma can be seen in Fig. 2B. The amplitude of this short pulse at different operating parameters is presented in Tables 1 and 2.

Influence of experimental conditions on H_2O_2 production

In these experiments, the influence of four parameters (e.g. water matrix, rotational speed, air flow rate, and discharge voltage) on generation of H_2O_2 in the RSC-PL device was investigated and optimal experimental conditions identified.

The effect of water matrix on H_2O_2 production at three rotational speeds is shown in Fig. 3A. Under all conditions, measurable concentrations of H_2O_2 confirm that $^{\bullet}OH$ formed in the gas phase are successfully transported into the liquid phase in the novel RSC-PL device, similar to our previous design [32]. In plasma systems, H_2O_2 is primarily produced through the recombination of two $^{\bullet}OH$ radicals, and its concentrations after 30 min of treatment typically range between 30–70 mg/L [41,42]. As a significant fraction of $^{\bullet}OH$ is initially produced in the gas phase, the detection of H_2O_2 in the treated liquid provides indirect evidence that reactive species effectively cross the gas–liquid interface [43]. The results further demonstrate that the water matrix influences H_2O_2 formation, as higher H_2O_2 concentrations were consistently determined in DW at all rotational speeds. For both matrices at all three rotational speeds, H_2O_2 levels increased linearly ($R^2 \geq 0.98$). In the case of DW from 6.4 mg/L to 9.9 mg/L, with production rates from 13.9 to 18.1 μM/pass, at 3000 and 10,800 rpms, respectively (Suppl. 5: Exps. 6 and 4). The lower H_2O_2 levels detected in TW are likely due to the presence of inorganic ions that can scavenge reactive species during plasma-cavitation treatment, thereby reducing the rate and extent of H_2O_2 formation [5,34]. The determined values fall within the same concentration range as those reported in the literature, except in the case of [34] where much higher values were determined (Suppl. 6). However, comparisons between studies must be interpreted with caution, as these are usually conducted under different experimental conditions (e.g., plasma type, batch or flow-through setup, water matrix, gas used for plasma ignition, sample volume, treatment time) and lack of data regarding energy consumption. To the authors' knowledge, no studies directly compared H_2O_2 formation in DW and TW, however, those investigating degradation of various dyes report lower removal efficacy in more complex water matrices [2,5,34], which they attributed to radical scavenging effect. Interestingly, the plasma power measurements indicate slightly higher power consumption (Table 3) in the case of TW compared to DW at all rotational speeds, most probably due to the higher TW conductivity.

The differences observed for selected rotor's rotational speeds indicate the complexity of the combined plasma-cavitation treatment. The

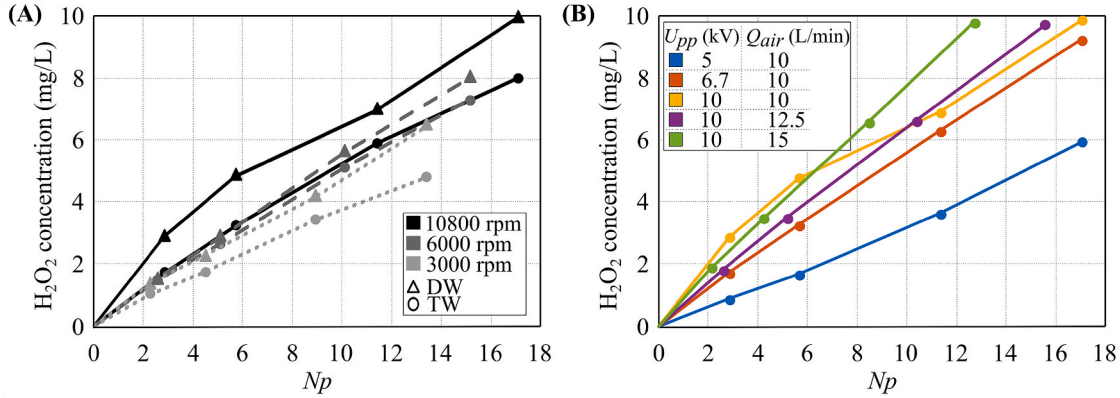

Fig. 3. Effect of water matrix (DW and TW) on the formation of H_2O_2 at three rotational speeds (10800, 6000, and 3000 rpm) at discharge voltage of 6.7 kV and an air flow of 10 L/min **(A)**. Effects of discharge voltage and air flow rate on the formation of H_2O_2 in DW at 10800 rpm **(B)**. All experiments were performed in 4 L samples and pulse repetition frequency of 10.8 kHz.

Table 3
Energy yield results, Y_{H2O2} and Y_{RR120}, at different operating conditions. The values were calculated for 15 min treatment time.

n (rpm)	Q_{air} (L/min)	*U* (kV)	P_{RSC} (W)	P_{PL} TW (W)	P_{PL} DW (W)	Y_{H2O2} *TW* (mg/Wh)	Y_{H2O2} *DW* (mg/Wh)	Y_{RR120} (mg/Wh) *100 mg/L*	Y_{RR120} (mg/Wh) *50 mg/L*	Y_{RR120} (mg/Wh) *25 mg/L*
3000	10	6.7	150	230	220	0.200	0.275	–	–	0.787
6000	10	6.7	260	235	225	0.233	0.261	–	–	0.581
10,800	10	6.7	450	240	235	0.184	0.231	1.817	0.832	0.405
10,800	10	4.1	450	–	200	–	0.227	–	–	–
10,800	10	3.0	450	–	150	–	0.159	–	–	–
10,800	12.5	6.7	440	–	235	–	0.231	–	–	–
10,800	15	6.7	430	–	235	–	0.236	–	–	–

rotor's rotational speed most probably influences gas–liquid mass transfer by forming more gas bubbles and promoting more frequent contact between gas phase and electrode surfaces. Enhanced gas dispersion and mixing increase the probability of local plasma ignition at each electrode, resulting in increased number and intensity of plasma events, i.e. micro discharges. Such behaviour is consistent with the observed increase in H_2O_2 production (Fig. 3A), as numerous and more energetic plasma events (Table 3: 240 W at 10800 rpm, compared to 235 W and 230 W at 6000 and 3000 rpm respectively) generate larger amounts of RONS. Furthermore, the results also show that increasing rotors' frequency influences also the system's oxidative intensity per pass, as H_2O_2 production rate per pass increases at higher rotor frequencies (most profoundly in the case of DW) (Suppl. 5). In parallel, slightly increased plasma power over rotor's frequency, for both TW and DW (Table 3) indicates that the plasma is operating at a higher intensity, which is consistent with the formation of stronger and more frequent local discharges. With increasing rotor frequency, the static pressure at the electrode outlet decreases, leading to the formation of larger gas bubbles before detachment which increases the active plasma volume and allows the plasma to remain ignited for a longer period.

Interestingly, despite higher plasma power measured in TW, the formation of H_2O_2 was lower compared to DW. Besides the effect of ionic scavengers, this discrepancy may also be linked to the higher electrical conductivity of TW (Section 3.1.3, Suppl. 7). Elevated conductivity can influence plasma behaviour shifting a greater portion of the input energy towards Joule heating of the liquid, thereby reducing the energy available for sustaining plasma discharges. Under such conditions, higher voltages are required to initiate and maintain constant plasma parameters, effectively decreasing the effectiveness of RONS generation and, consequently, limiting H_2O_2 accumulation in the liquid phase.

The effects of discharge voltage and air flow rate were evaluated in DW at 10800 rpm, as this condition yielded the highest H_2O_2 concentrations. As shown in Fig. 3B, H_2O_2 generation rose when discharge voltage increased from 3 to 4.1 and 6.7 kV. The trend aligns with previous studies reporting improved oxidation performance at higher discharge voltages, which is generally attributed to increased electron density and, consequently, enhanced production of reactive species [7,18,25,35]. As discharge voltage increased, power consumption rose as well (Table 3) indicating that more energy is being delivered into the discharge region. This increase in energy density promoted more frequent electron impact dissociation events, thereby driving higher radical yields [15,20]. Increasing air flow rate from 10 to 12.5 and 15 L/min did not influence H_2O_2 formation when comparison is based on treatment time (Suppl. 5: Exps. 4, 7 and 8). However, when comparison is made in *Np*, higher Q_{air} generally gives better results (Fig. 3B), since Q_{air} influences Q_{water}. Slightly higher H_2O_2 concentrations were observed when *Np* were lower than 6 at an air flow rate of 10 L/min compared to 12.5 and 15 L/min. Our results with increasing air flow rate (Suppl. 5) are comparable to the study performed by Mohammed et al., 2023 [7], where no difference was observed in degradation of dyes when the flow rate of Ar in plasma-only setup was investigated. However, Vaiano et al., 2022 [4] showed that the flow rate of O_2 influenced degradation of the investigated dye when plasma was combined with catalysis. In comparison with studies combining cavitation and plasma, our findings are consistent with results reported by [31]. They showed that the way in which the air bubbles are introduced into the acoustic cavitation field (using glass nozzles or porous plug) plays an important role. The increase of air flow rate (up to 8 L/min) through the glass nozzles, comparable to our design, showed no benefits on oxidation performance of their design. The reason for this could be the bubble size, which, at an increased air flow rate, limited both the residence time of bubbles in the discharge region and the surface area available for plasma-liquid interaction. Higher air volume at increased air flow rate could also contribute to discharge instability and reduce the effective energy density delivered to each bubble, preventing further increases in H_2O_2 formation.

Influence of experimental conditions on pH and conductivity

The effects of cavitation-plasma treatment on pH and conductivity in TW and DW are presented in Suppl. 7. Measured values of both parameters show considerable changes in experiments performed in DW (Suppl. 7: Exps. 4–10). The pH dropped from 5.9 down to 3.9, whereas the conductivity increased from 1.1 up to 77.7 μS/cm (Suppl. 7: Exp. 4). The pH values slowly decreased in all 7 experiments, which can be attributed to the formation of various nitrogen species accompanying atmospheric-pressure plasmas [19]. The presence of these species is evident from the recorded OES spectrum (Fig. 2). This was also observed in other studies where plasma was ignited in air and was independent of the plasma setup investigated. Allabakshi et al., 2023 [5] reported a drop of pH from 6.6 to 1.9 in 32 min, Liu et al., 2024 [1] showed a drop from 7.2 down to 3.7 in 10 min, Attri et al., 2016 recorded a decrease from 6.5 down to 5, whereas Rashid et al., 2020 [6] showed only a minor decrease from 7.5 down to 7.2. In accordance with our results (Suppl. 7: Exps. 1–3), no changes in pH values were reported by Tichonovas et al., 2013[8] and Vasikaran et al., 2022 [25] who performed experiments in TW. The reason could be in the buffer capacity of TW, where the presence of inorganic salts neutralizes nitrogen species formed during plasma, maintaining constant pH values.

Similar to the pH results, there were no changes in conductivity values measured in experiments performed in TW (Suppl. 7: Exps. 1–3), which is again in accordance with results reported by Tichonovas et al., 2013 [8] and Vasikaran et al., 2022 [25]. Contrary to this, the results of conductivity measurements in DW (Suppl. 7: Exps. 4–10) show a gradual increase for all experiments, which is most likely due to the increased production of NO_2^- and H^+ [6,19]. The increase is more pronounced in experiments performed at 10800 rpm (Suppl. 7: Exps. 4, 7, and 9) with the highest value (77.7 μS/cm) recorded at an air flow rate of 10 L/min and discharge voltage of 6.7 kV. These results correlate with the findings on H_2O_2 production (Fig. 3A) discussed in Section 3.1.2. Similar increase in conductivity, from 100 up to 135 μS/cm in 25 min, was reported by [6].

Influence of experimental conditions on dye decolorization

The results of RR120 decolorization at three different concentrations are presented in Fig. 4A. As expected, the removal effectiveness depends on the initial concentration, with higher removals observed at lower dye concentrations (up to 30 %), which is in agreement with other studies [7,15,25,35]. However, when the data are evaluated in terms of the

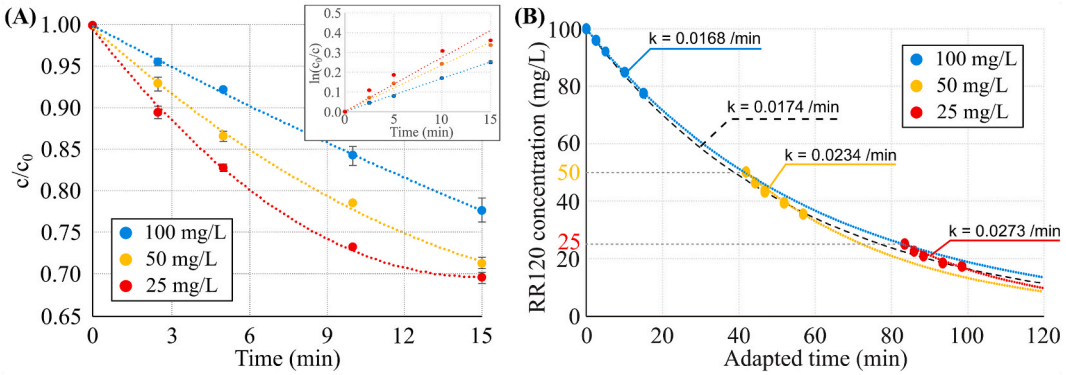

Fig. 4. Influence of RR120 concentration on the decolorization and reaction rate constants **(A)**. Concentration adjusted time profiles for RR120 at initial concentrations of 100, 50, and 25 mg/L. The black dashed trendline determines the overall exponential trend of all three concentrations. The colored dotted lines are trends for each individual set of measurements **(B)**. Experiments were performed in 4 L DW samples, at 10800 rpm, discharge voltage of 6.7 kV, and pulse repetition frequency of 10.8 kHz.

absolute mass of dye removed (mg/L), the highest decrease is achieved at the highest initial concentration (20.7 mg removed per L at 100 mg/L, compared to 7.7 mg removed per L in the case of 25 mg/L). This is reasonable as the production of reactive species in the cavitation-plasma treatment at selected experimental conditions is essentially constant. When these species are present in excess relative to the dye, as is indicated by the results of mass removed per L in our study, increasing the initial dye concentration allows more dye molecules to be oxidized, resulting in a higher amount of mass of the parent compound decolorized. This trend has likewise been reported in other plasma-based removal studies [30]. The very modest removal of the parent compound at all investigated concentrations (Fig. 4A) can be attributed to the physico-chemical properties of RR120, particularly its hydrophilic nature. The RR120 molecule has six sulfonic acid groups ($-SO_3H$), which are fully deprotonated at neutral pH and thus strongly hydrated, which results in the dye more likely remaining in the bulk solution. This type of dye was selected intentionally, as the goal of the study was to design a device capable of treating compounds that do not remain near the gas–liquid interface, where radical species are predominantly generated in both plasma and HC [19,23]. Demonstrating removal of hydrophilic compounds would suggest that the treatment is also effective for hydrophobic substances. As can be seen from the literature (Suppl. 8), numerous attempts of utilizing various plasma setups, either alone or in combination with cavitation have been investigated for the removal of different dyes. Control experiments (Suppl. 9) show that only minimal decolorization occurs with HC + H_2O_2 (Exp. C1), and no removal is observed when the dye is mixed with H_2O_2 alone (Exp. C2). This confirms that RR120 is largely removed when it encounters reactive species at the gas–liquid interface rather than long-lived oxidants like H_2O_2. Similar was reported for other azo dyes [3,11,15,18], where it was hypothesized that the azo bond is the first to be oxidized, forming various smaller intermediates, which are in the end broken down to CO_2, H_2O, SO_4^{2-} and NO_3^-. With the size of the RR120 (M = 1469.98 g/mol), one can assume that many different intermediates can be formed and remain in the solution due to the relatively short treatment time. This is clearly demonstrated in Fig. 4B and discussed below. Allabakshi et al., 2023 [5] showed that the azo dye molecules with larger molecular size require prolonged treatment times for removal of the initial molecule and even longer treatment times for mineralization. Liu et al., 2024 [1] reported that longer treatment times were needed to degrade methyl orange compared to methylene blue, which they ascribed to different molecular sizes and charge properties.

The RR120 decolorization exhibits apparent first-order behaviour (Fig. 4A), which is often observed in plasma discharge settings as the concentration of $^{\bullet}OH$ in the reactors is high and constant [2,20,25,34,35,44]. However, the observed reaction rate constant (k) is not independent of the initial dye concentration (Fig. 4A). Instead, the apparent first-order rate constant increases as the initial concentration decreases, indicating that the reaction does not follow a true first-order kinetics but rather concentration-dependent pseudo first-order behaviour [45]. The highest k value (0.0273/min) was determined at 25 mg/L (R^2 = 0.9711), which then dropped to 0.0234/min at 50 mg/L (R^2 = 0.9944) and further to 0.0168/min at 100 mg/L (R^2 = 0.997). This has also been reported in previous studies [15,25,35,44] and can be attributed to competition between the produced reactive species and the growing number of intermediate products formed at higher initial concentration. These intermediates most probably accumulate at the gas–liquid interface before migrating into the bulk solution, thereby reducing the availability of reactive species for target compounds [7,25,44]. Such inhibitory processes most likely occur immediately after the start of the treatment, leading to lower effective reaction rates in more concentrated samples. Consequently, the kinetics reflect not only the intrinsic radical generation rate but also the evolving competitive chemistry within the reaction medium.

The data on Fig. 4A at 100 and 50 mg/L are described by the apparent first-order kinetics model ($R^2 > 0.99$), a slight deterioration of the correlation is observed at 25 mg/L ($R^2 \approx 0.97$), where the relationship becomes visibly less linear. This (still small) deviation at low concentration is possibly related to a limiting fraction of the dye that is less accessible to cavitation-plasma generated reactive species. Nevertheless, the overall trends remain consistent with apparent first-order kinetics over the main part of the concentration range, with systematic deviations at low concentration supporting the presence of additional limiting or inhibitory processes. A noticeable additional decolorization during the rest period (from 22.2 % at 15 min to 27 % after 30 min) is observed only at the 100 mg/L concentration (Suppl. 10), while differences at other concentrations are essentially negligible. The most plausible explanation for this increased removal is that certain reactive species capable of interacting with the RR120 molecules remain in the samples after the cavitation-plasma treatment. However, because the likelihood of these species encountering and affecting dye molecules increases with dye concentration, the effect becomes detectible only at the highest investigated concentration. Nevertheless, more detailed studies of the species present after treatment are required to confirm this explanation.

To determine whether the parent compound undergoes mineralization TOC measurements are usually performed, however as the present study is only a proof of concept, this lies beyond its scope. An alternative approach to visualize whether the parent compound undergoes mineralization or whether intermediates are formed during degradation is given in Fig. 4B, which compiles the concentration–time data for all initial dye concentrations into a single diagram. Blue trendline for 100

mg/L was set as baseline, which was used to shift the original curves for 50 (yellow line) and 25 mg/L (red line) in time from 0 to 41.8 and 83.4 min, respectively. The time shift values were determined by assuming an overall exponential reduction trend and finding the least square difference. The overall exponential trend considering data from all three concentrations is plotted as black dashed line. We see that the trend for the $C_0 = 100$ mg/L closely follows the overall trend. On the other hand, the trends at lower initial concentrations predict somewhat faster reductions. In both cases, concentrations drop rapidly at early treatment times and faster than 100 mg/L sample would at these concentrations, likely indicating the formation of secondary reaction products that compete for reactive species and gradually diminish the effective decolorization rate.

Additionally, the results show that when the dye was added to the initial solution, the pH increased from 5.9 up to 7.1 (Suppl. 7: Exps. A–E, C1–C2), and then gradually decreased down to 3.9, like the values observed for the H_2O_2 production experiments (Exps. 4–10). The same was observed for the conductivity results, where the level of increase in conductivity depended on the initial dye concentrations. During the experiments, the conductivity gradually increased in all 5 experiments, reaching the highest value of 126.0 ± 1.8 at 100 mg/L of RR120 (Exp. A). This trend was also observed when plasma was used to investigate removal of other azo dyes [1,3,6]. During the rest period, the values remained constant, indicating that the remaining species do not influence these two parameters.

It can be seen from Fig. 5 that when 6000 and 3000 rpm were selected, the results of RR120 decolorization and kinetic constants are comparable. As the concentration of H_2O_2 increased with increasing rotational speed (Fig. 4A), these results indicate that the decolorization could also occur due to the presence of other radicals besides $^{\bullet}OH$. To confirm this, more studies are needed in the future. The pH and conductivity measurements (Suppl. 7: Exps. D–E) showed the same trends as in the case of Exps. A–C.

Influence of experimental conditions on energy consumption

Even though the research was performed on a laboratory scale, using a novel experimental device with priorities other than energy optimization, an energy analysis was performed (Table 3) to assess the efficiency of the novel cavitation-plasma device and its potential for further development. As numerous factors (e.g., rotational speed, discharge voltage, and initial dye concentration) influence the energy yield, the calculations were performed at all investigated experimental conditions. One must be aware that both, the cavitation device and the HV high-frequency plasma generator were neither designed nor optimized to operate at optimal energy efficiency. Separate electric powers are listed in Table 3 for both cavitation and plasma part, while energy yield results, due to the nature of the treatment device combine both, energy consumption of cavitation as well as plasma.

The power consumption of the cavitation unit was mostly affected by different rotational speeds and lower rpm values in general offered higher efficiency in terms of both Y_{H2O2} and Y_{RR120}. In case of higher air flow rates, the power consumption was mildly affected, and higher gas distribution slightly decreased its values (up to 5 %). The same trend observed in the case of H_2O_2 concentrations (Fig. 4A) can also be seen in energy yields, where higher values were always achieved in DW. In the case of TW, the highest Y_{H2O2} value (Table 3: 0.233 mg/kWh) was achieved at 6000 rpm, while in the case of DW, 3000 rpm seemed to be the most efficient (Table 3: 0.275 mg/kWh). Even though absolute values and production rates per pass in view of H_2O_2 production in TW and DW (Fig. 4A, Suppl. 5) generally show best results at higher rotational speeds, the energy yields are affected. Higher air flow resulted in no major differences in Y_{H2O2}. The power consumption for the plasma unit was strongly affected by discharge voltage, while water selection (TW/DW) and rotor's frequency had a mild but consistent influence. Plasma unit power was consistently higher in the case of TW (by up to 5 %) and rose with higher rotor's frequency (up to 6 %). The highest Y_{H2O2} were achieved at higher discharge voltages (Table 3: up to 0.275 mg/kWh at 6.7 kV). In the case of RR120, the highest Y_{RR120} values were achieved at higher initial concentrations from 1.817 mg/kWh at 100 mg/L down to 0.405 mg/kWh at 25 mg/L (Table 3). By lowering the initial concentration of the dye, the probability of an encounter between the pollutant molecules and reactive species also decreases, which ultimately negatively impacts the energy yield and has also been reported in the literature [18,30]. Furthermore, as the removals of the dye per pass at the concentration of 25 mg/L at different rotor's frequency (Fig. 5) did not differ, the highest Y_{RR120} was achieved at the lowest rotational speed (Table 3: 0.787 mg/kWh) due to the lowest energy consumption of the RSC-PL device.

Although numerous studies have investigated the removal of azo dyes using non-thermal atmospheric plasma and its combination with cavitation, these works differ substantially in their experimental conditions (Suppl. 8). Consequently, direct comparisons of removal yields should be interpreted with caution. It should also be noted that RR120 is a considerably larger molecule than most other azo dyes, making comparisons at equal initial concentrations difficult. Nevertheless, the comparison between the present study and the literature on the degradation of azo dyes with plasma and single cavitation-plasma research is given in the Suppl. 8.

Conclusions

This study presents a novel hybrid hydrodynamic cavitation and non-thermal plasma reactor with a systematic investigation on the treatment of azo dye Reactive Red 120 contaminated water, demonstrating both functional feasibility and its wastewater management. The main conclusions reached inside the study are as follows:

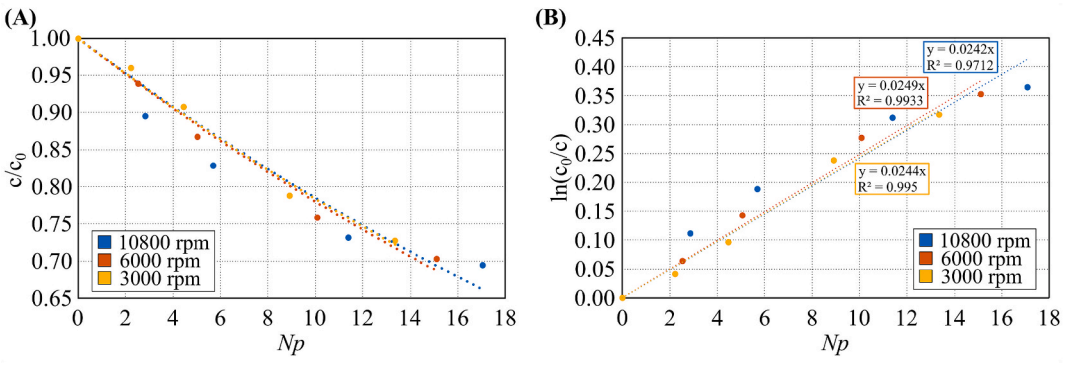

Fig. 5. Influence of rotational speed on RR120 decolorization **(A)** and reaction kinetics **(B)**. Experiments were performed in 4 L DW samples, at 25 mg/L of RR120, discharge voltage of 6.7 kV, air flow rate of 10 L/min and pulse repetition frequency of 10.8 kHz.

- The results showed that H_2O_2 formation are strongly influenced by the water matrix and operating conditions. Deionized water consistently gave higher oxidative capacity than tap water, highlighting the importance of inorganic radical scavengers in real wastewater systems.
- Increasing plasma discharge voltage, air flow rate and cavitation rotor speed enhanced reactive species generation, whereas lower rotational speeds improved energy efficiency, highlighting the trade-off between treatment intensity and overall energy performance.
- Reactive Red 120 decolorization followed apparent pseudo first-order kinetics, with rate constants decreasing at higher initial dye concentrations probably due to competition with intermediate by-products and limited accessibility of the hydrophilic dye at the gas–liquid interface.
- Control experiments confirmed that long-lived oxidants such as H_2O_2 alone were insufficient in the process of decolourization, emphasizing the dominant role of short-lived plasma- and cavitation-generated species.

The findings suggest further optimization of electrode configuration with gas distribution optimization and selection of desired cavitation conditions for higher oxidation efficiency. The novel device offers a new concept for a promising development of an advanced treatment process overcoming limitations of conventional methods. However, continuation of the research and device optimization is an essential step to advance the technology toward practical applications.

Declaration of Generative AI and AI-assisted technologies in the writing process

During the preparation of this work the authors used ChatGPT only to improve language and readability. After using this tool, the authors reviewed and edited the content as needed and take full responsibility for the content of the publication.

Data availability

Raw and analyzed data are available on Zenodo via web link: https://doi.org/10.5281/zenodo.18348661.

CRediT authorship contribution statement

Mojca Zupanc: Writing – review & editing, Writing – original draft, Investigation, Formal analysis, Data curation, Conceptualization. **Sebastian Dahle:** Writing – review & editing, Data curation, Conceptualization. **Matevž Dular:** Writing – review & editing, Formal analysis. **Gregor Primc:** Writing – review & editing, Resources, Formal analysis. **Rok Zaplotnik:** Writing – review & editing, Investigation, Formal analysis, Data curation. **Martin Petkovšek:** Writing – review & editing, Resources, Investigation, Funding acquisition.

Declaration of competing interest

The authors declare that they have no known competing financial interests or personal relationships that could have appeared to influence the work reported in this paper.

Acknowledgements

This work was supported by the Slovenian Research and Innovation Agency through Research Core Funding No. P2-0401, P2-0422, P2-0082, P4-0015 and Research Projects No. J2-4480, N2-0381, J2-60032, N2-0376 and Horizon Europe: 101248240 - ERC PoC PureWater. The authors would like to thank Ajda Novak and Meghan Grace Bohnert, master students, for contributing to the research through their Master thesis.

Appendix A. Supplementary material

Supplementary data to this article can be found online at https://doi.org/10.1016/j.jiec.2026.03.008.

References

[1] Q. Liu, J. Zhu, W. Ouyang, C. Ding, Z. Wu, K. (Ken) Ostrikov, Cold plasma turns mixed-dye-contaminated wastewater bio-safe, Environ. Res. 246 (2024). https://doi.org/10.1016/j.envres.2024.118125.
[2] H. Moradi, D.S. Kim, J.K. Yang, Y.Y. Chang, T. Kamranifard, Mechanistic study on the synergy of cold plasma and sulfate radical in the degradation of azo and triarylmethane dyes using density functional theory, J. Environ. Chem. Eng. 11 (2023), https://doi.org/10.1016/j.jece.2023.110559.
[3] S. Ma, S. Lee, K. Kim, J. Im, H. Jeon, Purification of organic pollutants in cationic thiazine and azo dye solutions using plasma-based advanced oxidation process via submerged multi-hole dielectric barrier discharge, Sep. Purif. Technol. 255 (2021), https://doi.org/10.1016/j.seppur.2020.117715.
[4] V. Vaiano, L.N. Miranda, G. Pepe, M.G. Basilicata, P. Campiglia, G. Iervolino, Catalytic non-thermal plasma process for the degradation of organic pollutants in aqueous solution, J. Environ. Chem. Eng. 10 (2022), https://doi.org/10.1016/j.jece.2022.107841.
[5] S.M. Allabakshi, P.S.N.S.R. Srikar, R.K. Gangwar, S.M. Maliyekkal, Treatment of azo, direct, and reactive dyes in surface dielectric barrier discharge: valorization of effluent, the influence of wastewater characteristics, and plasma modeling by Stark broadening technique, J. Water Process Eng. 56 (2023), https://doi.org/10.1016/j.jwpe.2023.104503.
[6] M.M. Rashid, M. Chowdhury, M.R. Talukder, Textile wastewater treatment by underwater parallel-multi-tube air discharge plasma jet, J. Environ. Chem. Eng. 8 (2020), https://doi.org/10.1016/j.jece.2020.104504.
[7] S.A. Mohammed, O.S.A. Al-Khazrajy, M. Abdallh, K.A. Aadim, A. Al-Mamari, H. Al-Owaisi, E. Yousif, Removal of dyes from aqueous solutions using non-thermal plasma, Environmental Processes 10 (2023), https://doi.org/10.1007/s40710-023-00677-0.
[8] M. Tichonovas, E. Krugly, V. Racys, R. Hippler, V. Kauneliene, I. Stasiulaitiene, D. Martuzevicius, Degradation of various textile dyes as wastewater pollutants under dielectric barrier discharge plasma treatment, Chem. Eng. J. 229 (2013) 9–19, https://doi.org/10.1016/j.cej.2013.05.095.
[9] I. Ben Amor, H. Hemmami, S. Zeghoud, W. Zahnit, G. Nedjoud, M.F. Ferhat, M. Messaoudi, Cold plasma technology in wastewater treatment: mechanisms, applications, and key challenges for organic pollutant removal, Int. J. Environ. Sci. Technol. (2025), https://doi.org/10.1007/s13762-025-06509-y.
[10] X. Zhou, Z. Guo, X. Tang, W. Wang, M. Wu, B. Song, Y. Xiang, Y. Li, W. Xiong, D. Huang, C. Zhou, Sulfate radical-based advanced oxidation processes for simultaneous removal of antibiotic-resistant bacteria and antibiotic resistance genes and the affecting factors, Chem. Eng. J. 498 (2024), https://doi.org/10.1016/j.cej.2024.155149.
[11] P. Attri, M. Yusupov, J.H. Park, L.P. Lingamdinne, J.R. Koduru, M. Shiratani, E. H. Choi, A. Bogaerts, Mechanism and comparison of needle-type non-thermal direct and indirect atmospheric pressure plasma jets on the degradation of dyes, Sci. Rep. 6 (2016), https://doi.org/10.1038/srep34419.
[12] Q. Chen, B. He, Y. Ma, X. Wang, Q. Xiong, J. Li, Q.H. Liu, Influence of the pH value on the degradation of an azo dye of methyl orange by air discharge plasma, Plasma Processes Polym. 16 (2019), https://doi.org/10.1002/ppap.201800152.
[13] K. Kyere-Yeboah, I.K. Bique, X. chen Qiao, Advances of non-thermal plasma discharge technology in degrading recalcitrant wastewater pollutants. A comprehensive review, Chemosphere 320 (2023). https://doi.org/10.1016/j.chemosphere.2023.138061.
[14] S. Das, A.P. Bhat, P.R. Gogate, Degradation of dyes using hydrodynamic cavitation: Process overview and cost estimation, J. Water Process Eng. 42 (2021), https://doi.org/10.1016/j.jwpe.2021.102126.
[15] Y. Song, S. Nie, H. Ji, T. Qin, Z. Ma, Degradation of methyl orange using hydrodynamic cavitation coupled with plasma oxidation and ultraviolet C, J. Clean. Prod. 467 (2024), https://doi.org/10.1016/j.jclepro.2024.142887.
[16] Y. Benito, S. Arrojo, G. Hauke, P. Vidal, Hydrodynamic Cavitation As a Low-cost AOPFor Wastewater Treatment: Preliminary ResultsAnd a New Design Approach, WIT Trans. Ecol. Environ. 80 (2005), https://doi.org/10.2495/WRM050501.
[17] R.C. Sanito, S.J. You, Y.F. Wang, Degradation of contaminants in plasma technology: an overview, J. Hazard. Mater. 424 (2022), https://doi.org/10.1016/j.jhazmat.2021.127390.
[18] M. Ansari, G. Moussavi, M.H. Ehrampoosh, S. Giannakis, A systematic review of non-thermal plasma (NTP) technologies for synthetic organic pollutants (SOPs) removal from water: recent advances in energy yield aspects as their key limiting factor, J. Water Process Eng. 51 (2023), https://doi.org/10.1016/j.jwpe.2022.103371.
[19] M. Lunder, S. Dahle, R. Fink, Cold Atmospheric Plasma for Water Disinfection: Mechanisms, Efficacy and Resistant Bacteria Inactivation, Plasma Processes Polym. 22 (2025), https://doi.org/10.1002/ppap.70050.
[20] R. Zhou, T. Zhang, R. Zhou, A. Mai-Prochnow, S.B. Ponraj, Z. Fang, H. Masood, J. Kananagh, D. McClure, D. Alam, K. (Ken) Ostrikov, P.J. Cullen, Underwater microplasma bubbles for efficient and simultaneous degradation of mixed dye pollutants, Science of the Total Environment 750 (2021). https://doi.org/10.1016/j.scitotenv.2020.142295.

[21] A. Kumar, V.K. Saini, Y. Huaccallo-Aguilar, S.F. Reinecke, U. Hampel, Characterization of reactive species in water induced by cold atmospheric air plasma: Experimental applications for industrial micropollutant removal from wastewater and seed germination, J. Environ. Chem. Eng. 13 (2025), https://doi.org/10.1016/j.jece.2025.117263.
[22] H. Zheng, Y. Zheng, J. Zhu, Recent developments in hydrodynamic cavitation reactors: cavitation mechanism, reactor design, and applications, Engineering 19 (2022) 180–198, https://doi.org/10.1016/j.eng.2022.04.027.
[23] M. Gągol, A. Przyjazny, G. Boczkaj, Wastewater treatment by means of advanced oxidation processes based on cavitation – a review, Chem. Eng. J. 338 (2018) 599–627, https://doi.org/10.1016/j.cej.2018.01.049.
[24] B. Wang, T. Wang, H. Su, A dye-methylene blue (MB)-degraded by hydrodynamic cavitation (HC) and combined with other oxidants, J. Environ. Chem. Eng. 10 (2022), https://doi.org/10.1016/j.jece.2022.107877.
[25] E.M. Vasikaran, P. Murugesan, J.A. Moses, C. Anandharamakrishnan, Performance of non-thermal plasma reactor for removal of organic and inorganic chemical residues in aqueous media, J. Electrostat. 115 (2022), https://doi.org/10.1016/j.elstat.2022.103671.
[26] A. Mai-Prochnow, R. Zhou, T. Zhang, K. (Ken) Ostrikov, S. Mugunthan, S.A. Rice, P.J. Cullen, Interactions of plasma-activated water with biofilms: inactivation, dispersal effects and mechanisms of action, NPJ Biofilms Microbiomes 7 (2021). https://doi.org/10.1038/s41522-020-00180-6.
[27] B. Maršálek, Š. Zezulka, E. Maršálková, F. Pochylý, P. Rudolf, Synergistic effects of trace concentrations of hydrogen peroxide used in a novel hydrodynamic cavitation device allows for selective removal of cyanobacteria, Chem. Eng. J. 382 (2020), https://doi.org/10.1016/j.cej.2019.122383.
[28] V.O. Abramov, A.V. Abramova, G. Cravotto, R.V. Nikonov, I.S. Fedulov, V. K. Ivanov, Flow-mode water treatment under simultaneous hydrodynamic cavitation and plasma, Ultrason. Sonochem. 70 (2021) 105323, https://doi.org/10.1016/j.ultsonch.2020.105323.
[29] K. Pournemati, A. Habibi-Yangjeh, Z. Salmanzadeh-Jamadi, A critical review on application of emerging hybrid cavitation–plasma technology for remediation of wastewater effluents, J. Water Process Eng. 67 (2024), https://doi.org/10.1016/j.jwpe.2024.106183.
[30] N. Shahsavari, X. Zhang, Microbubble-enhanced cold plasma activation for water decontamination: degradation dynamics and energy yield in relation to pollutant concentration, total volume and flow rate of water, J. Water Process Eng. 55 (2023), https://doi.org/10.1016/j.jwpe.2023.104169.
[31] Y. Xu, T. Yamamoto, D. Hariu, S. Komarov, Effect of gas injection on cavitation-assisted plasma treatment efficiency of wastewater, Ultrason. Sonochem. 83 (2022), https://doi.org/10.1016/j.ultsonch.2022.105941.
[32] M. Zupanc, G. Primc, M. Dular, M. Petkovšek, R. Roškar, R. Zaplotnik, J. Trontelj, Proof-of-concept for removing micropollutants through a combination of sub-atmospheric-pressure non-thermal plasma and hydrodynamic (super)cavitation, Ultrason. Sonochem. 111 (2024), https://doi.org/10.1016/j.ultsonch.2024.107110.
[33] T. Qin, S. Nie, H. Ji, Z. Xie, Synergistic degradation and degradation pathways of methylene blue by plasma process combined with cavitation impinging stream reactor based on hydrodynamic cavitation, J. Environ. Chem. Eng. 11 (2023), https://doi.org/10.1016/j.jece.2023.110356.
[34] T.C. Pereira, E.M.M. Flores, A.V. Abramova, F. Verdini, E. Calcio Gaudino, F. Bucciol, G. Cravotto, Simultaneous hydrodynamic cavitation and glow plasma discharge for the degradation of metronidazole in drinking water, Ultrason. Sonochem. 95 (2023), https://doi.org/10.1016/j.ultsonch.2023.106388.
[35] Y. Fang, D. Hariu, T. Yamamoto, S. Komarov, Acoustic cavitation assisted plasma for wastewater treatment: degradation of Rhodamine B in aqueous solution, Ultrason. Sonochem. 52 (2019) 318–325, https://doi.org/10.1016/j.ultsonch.2018.12.003.
[36] S. Nie, T. Qin, H. Ji, S. Nie, Z. Dai, Synergistic effect of hydrodynamic cavitation and plasma oxidation for the degradation of Rhodamine B dye wastewater, J. Water Process Eng. 49 (2022) 103022, https://doi.org/10.1016/j.jwpe.2022.103022.
[37] C. Kormann, D.W. Bahnemann, M.R. Hoffman, Photocatalytic production of hydrogen peroxides and organic peroxides in aqueous suspensions of titanium dioxide, zinc oxide, and desert sand, Environ. Sci. Technol. (1998).
[38] T. Czerwiec, F. Greer, D.B. Graves, Nitrogen dissociation in a low pressure cylindrical ICP discharge studied by actinometry and mass spectrometry, J. Phys. D Appl. Phys. 38 (2005) 4278–4289, https://doi.org/10.1088/0022-3727/38/24/003.
[39] N. Kawahara, E. Tomita, T. Nakayama, Y. Ikeda, A. Nishiyama, Spatial and Temporal Characteristics of Laser-induced Air Plasma, 2006.
[40] M. Zver, R. Zaplotnik, M. Mozetič, A. Vesel, A. Filipić, D. Dobnik, G. Primc, Characterization of low-pressure gaseous plasma radiation and its usage for inactivation of waterborne viruses, Sep. Purif. Technol. 354 (2025), https://doi.org/10.1016/j.seppur.2024.128691.
[41] R. Banaschik, P. Lukes, H. Jablonowski, M.U. Hammer, K.D. Weltmann, J.F. Kolb, Potential of pulsed corona discharges generated in water for the degradation of persistent pharmaceutical residues, Water Res. 84 (2015) 127–135, https://doi.org/10.1016/j.watres.2015.07.018.
[42] R.K. Singh, L. Philip, S. Ramanujam, Continuous flow pulse corona discharge reactor for the tertiary treatment of drinking water: insights on disinfection and emerging contaminants removal, Chem. Eng. J. 355 (2019) 269–278, https://doi.org/10.1016/j.cej.2018.08.109.
[43] N. Wardenier, P. Vanraes, A. Nikiforov, S.W.H. Van Hulle, C. Leys, Removal of micropollutants from water in a continuous-flow electrical discharge reactor, J. Hazard. Mater. 362 (2019) 238–245, https://doi.org/10.1016/j.jhazmat.2018.08.095.
[44] M. Choudhary, P. Sarkar, S. Kumar Sharma, A. Kajla, S. Neogi, Quantification of reactive species generated in pulsed electrical discharge plasma reactor and its application for 17α-ethinylestradiol degradation in different water matrices, Sep. Purif. Technol. 275 (2021), https://doi.org/10.1016/j.seppur.2021.119173.
[45] D.F. Ollis, Kinetics of photocatalyzed reactions: five lessons learned, Front. Chem. 6 (2018), https://doi.org/10.3389/fchem.2018.00378.